Materials Characterization 139 (2018) 446–451

Contents lists available at ScienceDirect

Materials Characterization

journal homepage: www.elsevier.com/locate/matchar

Recrystallization and martensitic transformation in nanometric grain size Cu-Al-Ni thin films grown by DC sputtering at room temperature

M.J. Morán[a,*], A.M. Condó[a,b], N. Haberkorn[a,b]

[a] Instituto Balseiro, Universidad Nacional de Cuyo & CNEA, 8400 San Carlos de Bariloche, Argentina
[b] Consejo Nacional de Investigaciones Científicas y Técnicas, Centro Atómico Bariloche, Av. Bustillo 9500, 8400 San Carlos de Bariloche, Argentina

ARTICLE INFO

Keywords:
Thin films
Microstructure
Shape memory

ABSTRACT

We report the recrystallization of metastable hexagonal and body centered cubic BCC phase in free-standing 6 μm thick Cu-Al-Ni films grown by DC sputtering at room temperature. The results show that the BCC phase recrystallizes to $L2_1$ at around 533 K *together* with precipitation of γ_2-phase. Annealing temperatures (533 K–623 K) at short times (0–30 min) produce systematic increment of the fraction of γ_2-phase. Films with phase coexistence of hexagonal, γ_2 and $L2_1$ structure display temperature driven martensitic transformation. This transformation is observed for samples with austenite grain size of around 30 nm. In all cases, the martensitic transformation temperature (M_S) notoriously decreases (compared to bulk) and systematically increases with the annealing temperatures and annealing time. In addition, the films display extended transformation and retransformation ranges along with asymmetric hysteresis, which may be associated to restitutive forces due to elastic deformations at martensite – martensite and martensite – austenite interfaces. Annealing temperatures above 623 K produce fast precipitation to equilibrium α- and γ_2-phases. The austenitic phase can be recovered after annealing over 1000 K and fast quenching in ice-water.

1. Introduction

Shape memory alloys are materials which present important reversible inelastic deformation, as a result of a thermoelastic martensitic transformation. Depending on temperature and material, strain which appears upon mechanical loading or cooling under stress is recovered after unloading and/or heating. The resulting effects, such as shape memory effect (SME), have potential applications in microactuators [1–3]. SME refers to the process of a sample which recovers its original shape after being deformed in the martensitic phase (by twin boundary motion) and then heated to the austenite phase. To enhance applications of SME at micro- or nano-scales, it is necessary to understand the role of dimension [4–6] and the microstructure [7–9] on martensitic transformations. In SMA thin films the dimension is usually related to the thickness t [10] and to the grain size D [11]. In addition, the martensitic transformation is also affected by chemical inhomogeneities [12], secondary phases [13] and topology [14].

Cu-based SMA are low-cost materials with a wide and tunable range of martensitic transformation temperatures (M_S). These materials include Cu-Zn, Cu-Al-Ni and Cu-Al-Zn, among others [15,16]. Cu-Al-Ni displays good mechanical performance in nano pillars [17] and in polycrystalline systems [18,19]. Cu-Al-Ni thin films are usually obtained by DC sputtering [20,21]. The deposition parameters are usually related to the temperature range of stability of bulk austenitic β-phase [22,23]. Thin films grown at low temperatures usually present metastable phases. For example, thin films grown at room temperature display a metastable disordered hexagonal (Hex) structure and body centered cubic (BCC) structures [20]. This metastable phases recrystallize to the equilibrium phases (α (Cu) and γ_2 (Cu_9Al_4)) above 600 K, and β-phase above 1000 K (depending on the chemical composition) [15,23,24]. In addition, thin films with metastable β-phase nanometric grains ($D \approx 150$ nm) and martensitic transformation can be obtained at deposition temperatures between 530 K and 590 K [21].

Here, we study the recrystallization and the martensitic transformation of free-standing 6 μm thick Cu-Al-Ni films grown at room temperature. Pristine films display nanometric grain size ($D \approx 30$ nm) with coexistence of BCC and Hex metastable phases. The films recrystallize during annealing at 563 K for 30 min (coexistence of Hex, $L2_1$ (austenite) and γ_2-phases). These films display martensitic transformation at M_S much lower than the one expected for bulk. The increment in the M_S value when the annealing temperature is increased to 623 K can be attributed to changes in the chemical composition due to precipitation of γ_2-phase. Nanometer grain sized films display an extended transformation range (M_S-M_F, being M_F the martensitic finish temperature)

* Corresponding author.
E-mail address: mjmoran@cab.cnea.gov.ar (M.J. Morán).

https://doi.org/10.1016/j.matchar.2018.03.025
Received 19 September 2017; Received in revised form 19 March 2018; Accepted 20 March 2018
Available online 21 March 2018

and large hysteresis ($\Delta h = A_F - M_S$, being A_F the austenitic finish temperature). This can be attributed to large elastic deformation at the interfaces between martensite – martensite, martensite – austenite and martensite – Hex/γ_2-nanoprecipitates. Either long annealing periods of time at 623 K or higher annealing temperatures induce the precipitation of both α and γ_2-phases. The $L2_1$ phase is recovered by quenching films annealed at temperatures over 1073 K.

2. Experimental

Cu-Al-Ni films with nominal thickness of 6 μm were grown by DC sputtering on Si (100) without intentional heating of the substrate in an atmosphere of 10 mTorr of argon with a power of 50 W. The pre-vacuum in the sputtering chamber was $\approx 1 \times 10^{-6}$ Torr. A target (diameter: 38 mm, height: 4 mm) with chemical composition Cu–27 at.% Al–5 at.% Ni ($Cu_{68}Al_{27}Ni_5$, $M_S^{bulk} \approx 250$ K) was prepared with pure metals melted in an encapsulated quartz tube under argon atmosphere. During the deposition, the substrate was located at approximately 70 mm over the target. Deposition sputtering (growth rate of ~50 nm/min) was estimated from cross-section scanning electron microscope images (not shown). After grown, the Cu-Al-Ni films were easily peeled-off from the substrate and cut into pieces. The samples were successively annealed in air at 533 K for 30 min [533 K-30 m], 563 K for 30 min [563 K-30 m], 593 K for 15 min [593 K-15 m], and 623 K for 15 min [623 K-15 m]. In addition, [623 K-15 m] was encapsulated in quartz tubes under argon atmosphere inside a tantalum envelope and annealed at 1123 K for 20 min [1123 K-20 m]. Then, the sample was quenched in ice water [20].

The structure of the films was studied by transmission electron microscopy (TEM) with a TEM CM200 UT and a TEM FEI Tecnai F20. TEM specimens were prepared using standard ion milling techniques in a Gatan PIP system. The films were characterized by X-ray diffraction (XRD) in a Panalytical Empyrean equipment. The martensitic transformation was characterized by electrical transport using conventional four-probe geometry.

3. Results and Discussion

The microstructure of Cu-Al-Ni thin films grown at room temperature was previously discussed in ref. [20]. The microstructure displays nanometric grains with metastable Hex and BCC phases. The films are textured along (0002) and $(10\bar{1}0)$ in the Hex structure, whereas in the BCC structure the films are textured along (110) [20]. Fig. 1a–e show the XRD data corresponding to a pristine and to annealed films. The peaks correspond to multiple overlapping reflections and they were deconvoluted using Voigt functions. Pristine samples (Fig. 1a) show three different contributions corresponding to the $(0002)_{Hex}$, $(10\bar{1}0)_{Hex}$ and $(110)_{BCC}$ orientations. Fig. 1b shows the XRD pattern corresponding to [533 K-30 m]. The peaks can be fitted using narrower peaks, which may be attributed to slight changes in the grain size D and to a reduction strain generated during fabrication of the thin film. In addition, the peak corresponding to the $(110)_{BCC}$ orientation shifts to higher angles ($\approx 0.4^\circ$) and its intensity increases, which can be attributed to the recrystallization from BCC → $L2_1$ ($(220)_{L2_1}$). From this shift, and assuming a lattice parameter $a_{L21} = 0.5836$ nm for the $L2_1$ structure in Cu-Al-Ni alloys [25], we obtain a lattice parameter $a_{BCC} = 0.295$ nm for the BCC structure, in agreement with [21]. Fig. 1c shows the XRD pattern corresponding to [563 K-30 m]. A new peak emerges at approximately $2\theta = 44.2^\circ$, and it corresponds to (330) reflection of the γ_2-phase (Cu_9Al_4). When the film is annealed at higher temperatures, [593 K-15 m] and [623 K-15 m] (Fig. 1d,e), the peak corresponding to the $(330)_{\gamma 2}$ reflection increases, indicating changes in the microstructure associated to γ_2-precipitates. The peaks corresponding to the metastable Hex phase ($(0002)_{Hex}$ and $(10\bar{1}0)_{Hex}$) remain, even at 623 K. Samples annealed at 623 K for > 15 min or samples annealed at higher temperatures, are so extremely fragile (due to

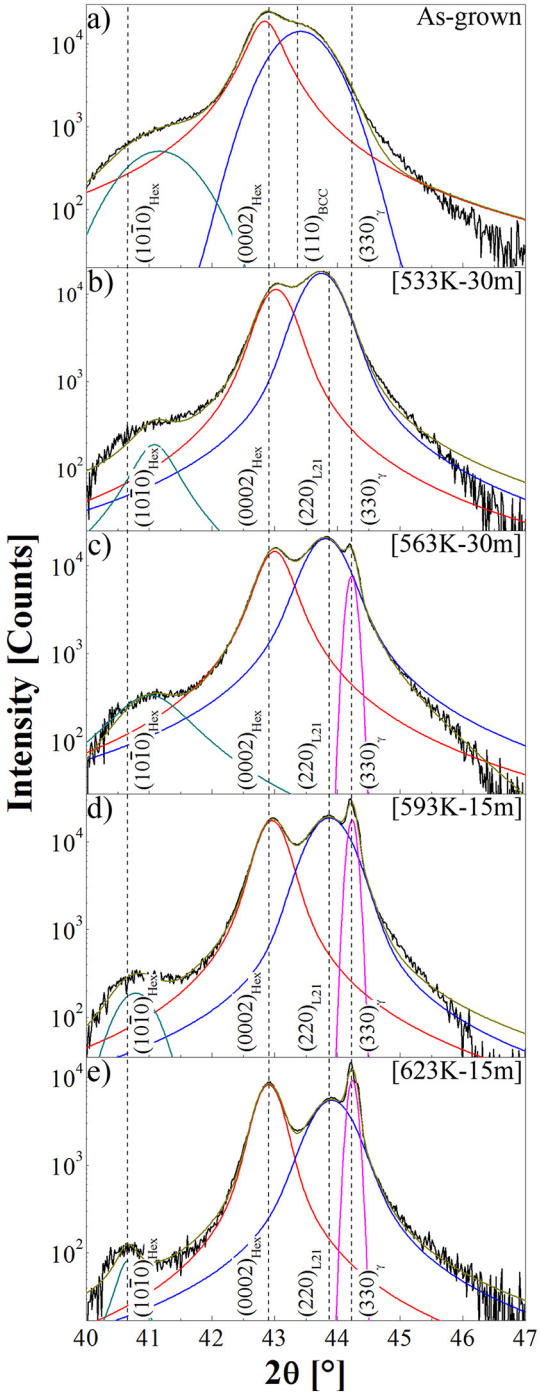

Fig. 1. X-ray diffraction patterns at room temperature of: a) As-grown Cu-Al-Ni film; b) [533 K-30 m]; c) [563 K-30 m]; d) [593 K-15 m]; e) [623 K-15 m]. The peaks were indexed by considering BCC, γ_2-phase, hexagonal disordered (Hex) and β-phase with $L2_1$ structure.

γ_2–phase precipitates), that their manipulation is impossible. The $L2_1$ structure is recovered for samples annealed at temperatures higher than 1073 K.

Fig. 2a–c show bright field plan-view TEM images corresponding to a pristine film, [563 K-30 m] and [623 K-15 m], respectively. Fig. 2d–f show the corresponding selected area electron diffraction (SAED) patterns. Fig. 2a shows a complex microstructure with a median of $\widetilde{D} \approx 30$ nm (see Fig. 3). The SAED pattern corresponds to all the expected reflection rings corresponding to the Hex and BCC structures (see Fig. 2d). Fig. 2b–c show large grains ($D \approx 150$–200 nm) embedded

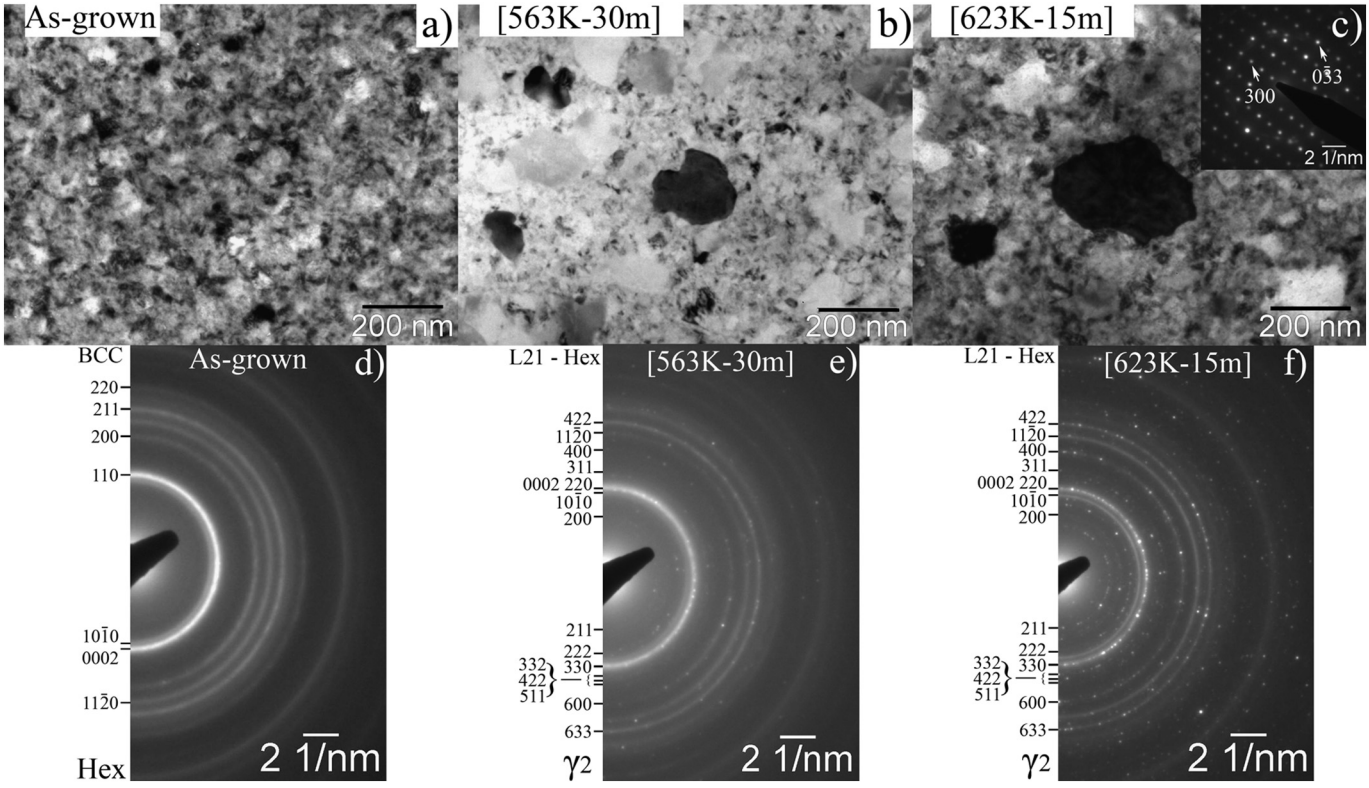

Fig. 2. a–c) Plan view bright field TEM image of an as-grown Cu-Al-Ni film, [563 K-30 m] and [623 K-15 m], respectively. Inset in Fig. 2c corresponds to γ_2 phase [011] zone axis. d–f) Electron diffraction patterns corresponding to an as-grown Cu-Al-Ni film, [563 K-30 m] and [623 K-15 m], respectively.

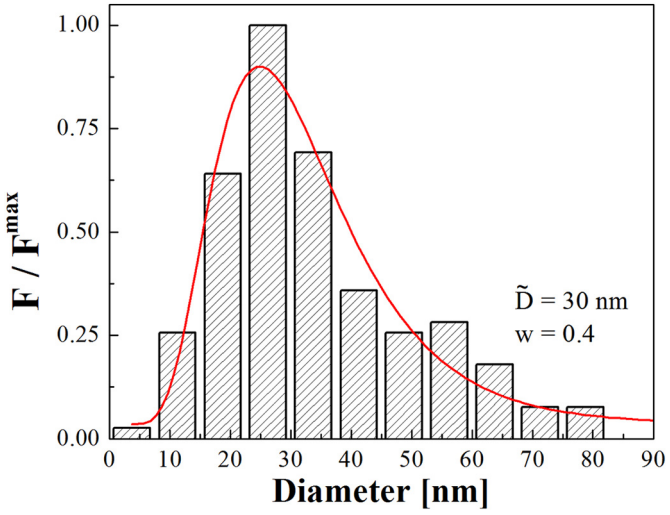

Fig. 3. Grain size histogram and its log-normal fitting for Cu-Al-Ni films deposited at room temperature.

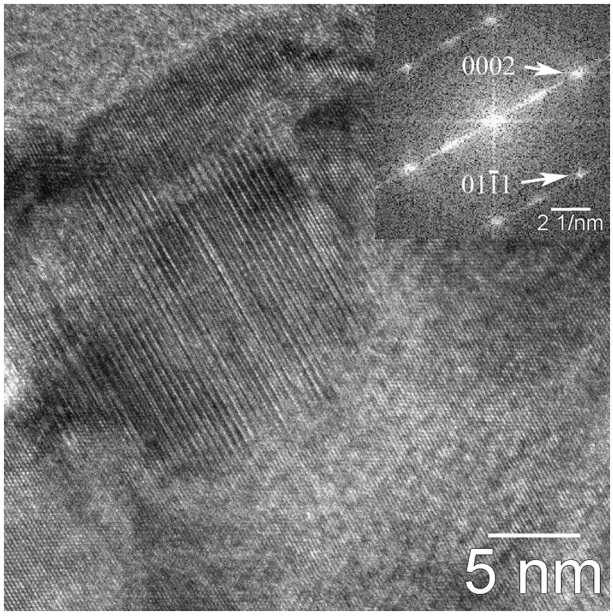

Fig. 4. High resolution TEM image of [593 K-30 m] showing a nanometric grain of the hexagonal phase. Inset shows the Fast Fourier transformation of the grain. The image was obtained along the $[2\bar{1}\bar{1}0]$ zone axis direction.

in a matrix with small sized grains (30 nm). As identified in inset Fig. 2c, these large grains correspond to the γ_2–phase (cubic structure of stoichiometry Cu_9Al_4). In the SAED patterns corresponding to [563 K-30 m] and [623 K-15 m], the rings can be indexed considering Hex, $L2_1$ and γ_2–phase, which is in agreement with the XRD data shown in Fig. 1. The rings corresponding to $L2_1$ and Hex structures are uniform (small grain size), whereas those corresponding to the gamma phase show only some reflections (larger grain size). It is worth mentioning that the increment in the $(330)_{\gamma 2}$ narrow reflection observed for annealed samples in Fig. 1c–e can be attributed to large γ_2 precipitates. Moreover, in the recrystallization of Cu-Al-Ni thin films grown at room temperature the Hex phase remains at temperatures up to 623 K. The small size of the Hex grains is evidenced by wider peak widths for the $(0002)_{Hex}$ and $(10\bar{1}0)_{Hex}$ reflections. Fig. 4 shows a high resolution TEM image corresponding to [593 K-30 m]. The grain shows a characteristic modulation that can be associated to a small grain of the Hex phase ($D \approx 15$ nm), which is showed in the Fast Fourier transformation (see inset Fig. 4).

To verify the existence of martensitic transformation in the films,

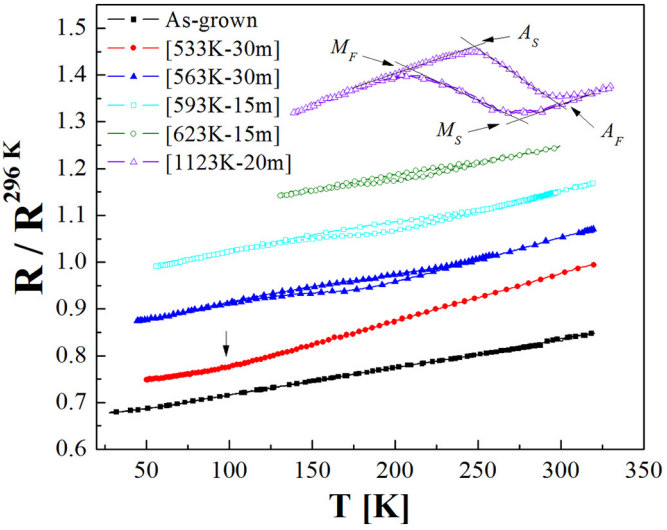

Fig. 5. Normalized resistance (R/R^{296K}) versus temperature for the as-grown Cu-Al-Ni film, [533 K-30 m], [563 K-30 m], [593 K-15 m], [623 K-15 m] and [1123 K-20 m]. The normalized resistance graphs are shifted for a clearer presentation.

Table 1
Characteristic temperatures for annealed Cu-Al-Ni thin films.

Sample	M_S [K]	M_F [K]	A_S [K]	A_F [K]	A_F - M_S [K]
[563 K-30 m]	183 ± 5	112 ± 6	134 ± 9	241 ± 5	58 ± 10
[593 K-15 m]	198 ± 7	138 ± 7	174 ± 9	254 ± 6	56 ± 10
[623 K-15 m]	212 ± 3	156 ± 4	199 ± 6	267 ± 6	55 ± 9
[1123 K-20 m]	275 ± 2	209 ± 1	247 ± 2	299 ± 2	24 ± 4

electrical resistance (R) vs temperature (T) measurements were performed. Martensitic transformations are characterized by four representative temperatures: martensite start (M_S), martensite finish (M_F), austenite start (A_S) and austenite finish (A_F). Fig. 5 shows a summary of the results obtained. Table 1 displays a summary of the characteristic temperatures. The hysteresis width ($\Delta h = A_F - M_S$) is also included. The pristine sample does not present any features that could be associated with a martensitic transformation. Although a small break up at around 100 K appears when the sample is annealed at [533 K-30 m], no hysteresis is observed in the cooling down and warming up curves. This suggests that the martensitic transition is strongly affected by the strained grain boundaries. Hysteresis is, however, observed for the martensitic transformation corresponding to samples with higher annealing temperatures ([563 K-30 m], [593 K-15 m] and [623 K-15 m]). In addition, the M_S of the transition systematically shifts to higher temperatures when the annealing temperature is increased. For example, $M_S \approx 183$ K for [563 K-30 m] and $M_S \approx 212$ K for [623 K-15 m] (see Table 1). The systematic increment of M_S in the annealed films can be attributed to two different effects: changes in the matrix composition produced by the gradual γ_2 precipitation, which shift the M_S to higher values [15,26], and changes in the order of the $L2_1$ produced by an increment in the diffusion, which is evidenced in the presence of γ_2 nanoprecipitates [27]. In all cases, the M_S values for samples annealed at low temperatures (below 623 K) are smaller than that obtained for [1123 K-20 m]. The latter displays $M_S \approx 275$ K, which is close to the value expected for bulk specimens (differences are related to small changes in chemical composition [20]). In addition, the martensitic transformation in [1123 K-20 m] corresponds to $L2_1 \rightarrow$ 18R martensite [28], which is evidenced from XRD and TEM analysis (Fig. 6a,b). [1123 K-20 m] possess micrometric grains and martensite plates ranging from 200 nm to 600 nm wide, which are much larger than the grains corresponding to samples annealed at low

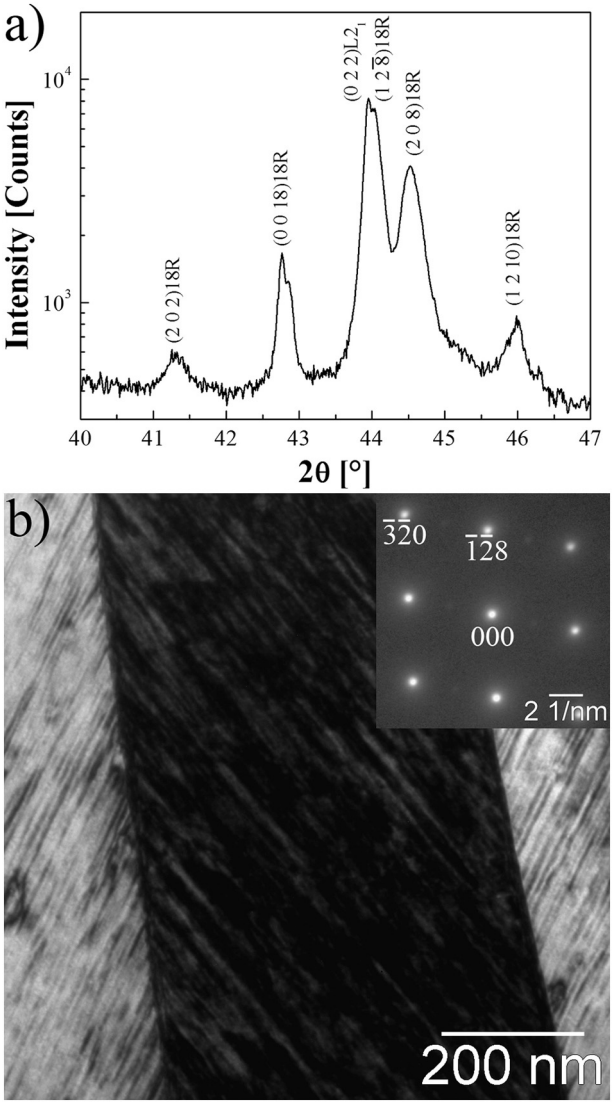

Fig. 6. a) X-ray diffraction patterns at room temperature of [1123 K-20 m] (after warming up the film from liquid N_2 temperature). b) Plan-view bright field TEM image in [1123 K-20 m] showing 18R twinned martensite. Inset shows the electron diffraction pattern along the $[4\bar{6}\bar{1}]$ direction corresponding to the dark central 18R plate.

temperatures. The martensitic transformation observed in the films annealed at low temperatures displays, in comparison with [1123 K-20 m], a suppressed jump in the resistivity. In addition, the films display extended transformation and retransformation ranges along with asymmetric hysteresis. These suggest that the martensitic transformation is partially blocked, which could be related to the presence of secondary phases (Hex and γ_2–grains) or to with an incomplete $L2_1 \rightarrow$ 18R transformation. Fig. 7 shows a comparison between XRD patterns obtained at room temperature (above the transformation) and 130 K (below the transformation) for [593 K-15 m]. The results show that the $(220)_{L2_1}$ reflection decreases at low temperatures and that reflections which may be related with $(12\bar{8})_{18R}$and $(208)_{18R}$ emerge in the pattern (similar features are observed in [623 K-15 m]), which indicates that a non-negligible volume of austenite transforms to martensite.

The outstanding feature in the recrystallization of Cu-Al-Ni thin films is the presence of martensitic transformation in samples with grain size around 30 nm. This size is below the limit reported for thin films and bulk specimens [20,21]. The temperature-driven martensitic transformation observed in films with $D \approx 30$ nm is strongly affected by the microstructure and it presents different transformation –

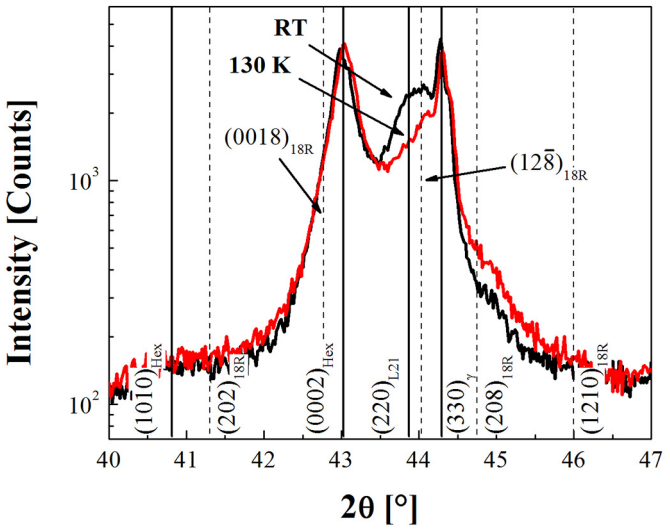

Fig. 7. X-ray diffraction patterns at room temperature and at 130 K for [593 K-15 m]. The expected reflections for Hex, γ_2, $L2_1$ and 18R phases are indicated.

retransformation temperature ranges (M_S-M_F and A_S-A_F), which is evidenced in the absence of a temperature clear break for A_S. M_S is strongly shifted to low temperatures in comparison with bulk specimens. Another relevant difference between films annealed at low temperatures and 1123 K is related to the suppressed change in the resistivity between austenite and martensite phases. These features can be related to stress at the interfaces in which $L2_1$ grains with different orientations coexist with Hex and γ_2 nanoprecipitates. In addition, incomplete martensitic transformation is inferred from XRD patterns at low temperatures. Usually, extended martensitic transformation range with narrow hysteresis (in comparison with bulk austenite) is observed in very thin films [10] and in bulk specimens, in which nanoprecipitates induce restoring forces on the martensitic domains [29]. Different energies are involved in thermal induced martensitic transformations in which the driving force is given by the chemical free energy ($\Delta G^{chem} = \Delta H - T\Delta S$; being ΔH the enthalpy and ΔS the entropy) [31]. This force ΔG^{chem} (generated by undercooling around T_0) is related to the $\Delta S^{L21\rightarrow 18R}$ and it can be estimated as $\partial \Delta G/\partial T = -\Delta S$. The $\Delta S^{L21\rightarrow 18R}$ in bulk Cu-Al-Ni is $\approx -2 \times 10^5\,J\,K^{-1}\,m^{-3}$ [30]. In comparison with [1123 K-20 min] ($T_0 = (M_S + A_F)/2 \approx 285$ K), the undercooling for films annealed at low temperatures (563 K–623 K) is ≈80 K, which corresponds to energy barriers (E^T) $\approx 1.6 \times 10^7\,J\,m^{-3}$. During thermal cycling (without applied stress), the change in the rate of Gibbs free energy density (i.e. per unit volume) can be defined as [5]:

$$\dot{G}_{A\leftrightarrow M} = [\Delta G^{ch} + \gamma_i A_i + \Delta\gamma_{sf} A_{sf} + E_{el}]\dot{f}_M + E_{fr}\,|\dot{f}_M| \quad (1)$$

where $\dot{f}_M$ is the rate of martensite volume fraction ($\dot{f}_M > 0$ during forward transformation and < 0 during reverse transformation), ΔG^{ch} changes sign at T_0, γ_i is the interfacial energy per unit area and A_i is the interfacial area density. The interfacial energies involved are the grain boundary attained by martensite plates (γ_{gb}), the interfaces between austenite and martensite plates (γ_{am}), and the twin interfaces within martensite plates (γ_{tw}) [31]. $\Delta\gamma_{sf} = \gamma_{sf}{}^M - \gamma_{sf}{}^A$ is the difference in surface energy per unit area of martensite and austenite, and multiplies the specific sample surface area A_{sf}. E_{el} is the average increment in the elastic energy density as a result of the transformation. The changes in chemical, interfacial surface and stored elastic strain energy are all recovered during reverse transformation, when $\dot{f}_M$ changes its sign. E_{fr} is the irreversible part of the free energy change, and is usually ascribed to frictional work produced by motion of interfaces. In polycrystalline SMA the nucleation and growth of the martensite plates are controlled by austenite grain boundaries [19]. The martensite plate thickness (h_{plate}) decreases as D is reduced [19]. Usually a domain of parallel plates is usually observed in grains smaller than 10 μm and $h_{plate} \approx 0.36\,D$ [19]. The h_{plate} typically observed in thin Cu-based SMA with 18R structure is much larger than 30 nm (see Fig. 6b). This suggests that the $L2_1 \rightarrow$ 18R transformation in nanograin sized Cu-Al-Ni thin films takes places with a single plate per grain. Unlike bulk and thin films with larger grain size [21,32], most energy is accumulated at grain boundaries (austenite – martensite, martensite – precipitate and martensite – martensite interfaces). The term E_{el} in Eq. (1) should accumulate energy (restorative force), which would contribute to reduce the hysteresis in the martensite – austenite retransformation ($A_S - M_F$). TEM images (including martensite structures) are necessary for a more detailed analysis of the barriers involved in the transformation.

4. Conclusions

The recrystallization of metastable Hex and BCC phases in free-standing 6 μm thick Cu-Al-Ni films grown by DC sputtering at room temperature is reported. The results show that metastable BCC recrystallize in $L2_1$ structure at low temperatures, whereas the Hex remains stable at temperatures up to 623 K. The films recrystallized at low temperatures (563 K and 623 K) show $L2_1$ grains with an average size of approximately 30 nm. Compared to bulk specimens, these films present thermal induced martensitic transformation at lower temperatures, which can be attributed to stress at grain boundaries due to variant accommodation, chemical gradients and phase coexistence. Samples with grain size ~30 nm are below the limit where martensitic transformation was reported for the Cu-Al-Ni alloy.

Acknowledgments

We thank to C. Gómez Bastidas, A. Geraci, M. Isla, M. Corte, C. Ramos and E. Aburto, for technical assistance. Financial support from ANCYPT PICT 2012-0884. N. H is member of the Instituto de Nanociencia y Nanotecnología (CNEA, Argentina).

References

[1] P. Krulevitch, A.P. Lee, P.B. Ramsey, J.C. Trevino, J. Hamilton, M.A. Northrup, Thin film shape memory alloy microactuators, J. Microelectromech. Syst. 5 (1996) 270–282.
[2] E. Pengwang, K. Rabenorosoa, M. Rakotondrabe, N. Andreff, Scanning micromirror platform based on MEMS technology for medical application, Micromachines 7 (2016) 24–53.
[3] S.A. Wilson, et al., New materials for micro-scale sensors and actuators: an engineering review, Mater. Sci. Eng. R 56 (2007) 1–129.
[4] C.P. Frick, S. Orso, E. Arzt, Loss of pseudoelasticity in nickel-titanium sub-micron compression pillars, Acta Mater. 55 (2007) 3845–3855.
[5] Y. Chen, C.A. Schuh, Size effects in shape memory alloy microwires, Acta Mater. 59 (2011) 537–553.
[6] J. San Juan, M.L. Nó, C.A. Schuh, Nanoscale shape-memory alloys for ultrahigh mechanical damping, Nat. Nanotechnol. 4 (2009) 415–419.
[7] T. Waitz, W. Pranger, T. Antretter, F.D. Fischer, H.P. Karnthaler, Competing accommodation mechanisms of the martensite in nanocrystalline NiTi shape memory alloys, Mater. Sci. Eng. A 481-482 (2008) 479–483.
[8] T. Lehnert, H. Grimmer, P. Böni, M. Horisberger, R. Gotthard, Characterization of shape-memory alloy thin films made up from sputter-deposited Ni/Ti multilayers, Acta Mater. 48 (2000) 4065–4071.
[9] A. Ishida, M. Sato, Microstructure and shape memory behaviour of annealed $Ti_{51.5}Ni_{(48.5-x)}Cu_x$ (x = 6.5 − 20.9) thin films, Philos. Mag. 87 (2007) 5523–5538.
[10] D. König, P.J.S. Buenconsejo, D. Grochla, S. Hamann, J. Pfetzing-Micklich, A. Ludwig, Thickness-dependence of the B2–B19 martensitic transformation in nanoscale shape memory alloy thin films: zero-hysteresis in 75 nm thick $Ti_{51}Ni_{38}Cu_{11}$ thin films, Acta Mater. 60 (2012) 306–313.
[11] A. Kumar, D. Singh, D. Kau, Grain size effect on structural, electrical and mechanical properties of NiTi thin films deposited by magnetron co-sputtering, Surf. Coat. Technol. 203 (2009) 1596–1603.
[12] P. Machain, A.M. Condó, P. Domenichini, G. Pozo López, M. Sirena, V.F. Correa, N. Haberkorn, Martensitic transformation in as-grown and annealed near-stoichiometric epitaxial Ni_2MnGa thin films, Philos. Mag. 95 (2015) 2527–2538.
[13] F.C. Lovey, V. Torra, Shape memory in Cu-based alloys: phenomenological behavior at the mesoscale level and interaction of martensitic transformation with structural defects in Cu-Zn-Al, Prog. Mater. Sci. 44 (1999) 189–289.
[14] S.M. Ueland, C.A. Schuh, Surface roughness-controlled superelastic hysteresis in shape memory microwires, Scr. Mater. 82 (2014) 1–4.

[15] V. Recarte, R.B. Pérez-Sáez, E.H. Bocanegra, M.L. Nó, J. San Juan, Dependence of the martensitic transformation characteristics on concentration in Cu-Al-Ni shape memory alloys, Mater. Sci. Eng. A 273–275 (1999) 380–384.
[16] M. Ahlers, Martensite and equilibrium phases in CuZn and CuZnAl alloys, Prog. Mater. Sci. 30 (1986) 135–186.
[17] J. San Juan, M.L. Nó, C.A. Schuh, Superelasticity and shape memory in micro- and nanometer-scale pillars, Adv. Mater. 20 (2008) 272–278.
[18] K. Mukunthan, L.C. Brown, Preparation and properties of fine grain β-CuAlNi strain-memory alloys, Metall. Trans. A. 19A (1988) 2921–2929.
[19] P. La Roca, L. Isola, Ph. Vermaut, J. Malarria, Relationship between martensitic plate size and austenitic grain size in martensitic transformations, Appl. Phys. Lett. 106 (2015) 221903–221906.
[20] C. Espinoza Torres, A.M. Condó, N. Haberkorn, E. Zelaya, D. Schryvers, J. Guimpel, F.C. Lovey, Structures in textured Cu–Al–Ni shape memory thin films grown by sputtering, Mater. Charact. 96 (2014) 256–262.
[21] M.J. Morán, A.M. Condó, F. Soldera, M. Sirena, N. Haberkorn, Martensitic transformation in freestanding and supported Cu-Al-Ni thin films obtained at low deposition temperatures, Mater. Lett. 184 (2016) 177–180.
[22] G. Petzow, G. Effenberg, Ternary alloys 5, VCH, N. Y. (1992) 615–625.
[23] J.I. Perez-Landazábal, V. Recarte, V. Sanchez-Alarcos, M.L. Nó, J. San Juan, Study of the stability and decomposition process of the β phase in Cu-Al-Ni shape memory alloys, Mater. Sci. Eng. A 438-440 (2006) 734–737.
[24] M. Hansen, Constitution of Binary Alloys, 2nd ed., McGraw-Hill, New York (NY), 1958.
[25] P. Molnár, P. Šittner, V. Novák, P. Lukáš, Twinning processes in Cu-Al-Ni martensite single crystals investigated by neutron single crystal diffraction method, Mater. Sci. Eng. A 481–482 (2008) 513–517.
[26] K. Wasa, Sputtering Phenomena, Second Edition, Elsevier Inc, 2012.
[27] R. Gastien, C.E. Corbellani, P.B. Bozzano, M.L. Sade, F.C. Lovey, Low temperature isothermal ageing in shape memory CuAlNi single crystals, J. Alloys Compd. 495 (2010) 428–431.
[28] S. Saud, E. Hamzah, T. Abubakar, H.R. Bakhsheshi-Rad, Thermal aging behavior in Cu-Al-Ni-xCo shape memory alloys, J. Therm. Anal. Calorim. 119 (2015) 1273–1284.
[29] P. La Roca, A. Baruj, C.E. Sobrero, J.A. Malarría, M. Sade, Nanoprecipitation effects on phase stability of Fe-Mn-Al-Ni alloys, J. Alloys Compd. 708 (2017) 422–427.
[30] R. Romero, J.L. Pelegrina, Change of entropy in the martensitic transformation and its dependence in Cu-based shape memory alloys, Mater. Sci. Eng. A 354 (2003) 243–254.
[31] H. Petryk, S. Stupkiewicz, G. Maciejewski, Interfacial energy and dissipation in martensitic phase transformations, part II: size effects in pseudoelasticity, interfacial energy and dissipation in martensitic phase transformations. Part II: size effects in pseudoelasticity, J. Mech. Phys. Solids 58 (2010) 373–389.
[32] P. Domenichini, A.M. Condó, F. Soldera, M. Sirena, N. Haberkorn, Influence of the microstructure on the resulting 18R martensitic transformation of polycrystalline Cu-Al-Zn thin films obtained by sputtering and reactive annealing, Mater. Charact. 114 (2016) 289–295.